Fiber-Chip Link via Mode Division Multiplexing

Oscar A. Jimenez Gordillo[ID], Asher Novick[ID], *Member, IEEE*, Oliver L. Wang[ID],
Anthony J. Rizzo[ID], Utsav D. Dave, Keren Bergman, *Fellow, IEEE*,
and Michal Lipson, *Fellow, IEEE*

Abstract— **Applying mode division multiplexing techniques to a fiber-chip link would greatly increase its communication bandwidth. However, its implementation is difficult due to the huge higher-order mode mismatch between multimode-integrated waveguides and optical few-mode fibers (FMF). Here, we present an integrated coupler between the higher-order modes of a silicon waveguide and those of a FMF. Our device is capable of terabit-per-second bandwidth based on the multiplexing of 4 spatial modes. It relies on a multi-stage silicon taper combined with a 3D polymer waveguide, which convert and shape the modes for one-to-one mode coupling to the FMF. We demonstrate an average crosstalk of −7 dB to the closest mode and capability for up to 1.92 Tb/sec data transmission in the L-band via mode and wavelength division multiplexing.**

Index Terms— **Optical waveguides, optical fiber couplers, photonic integrated circuits, space division multiplexing, 3D printing.**

I. INTRODUCTION

MODE division multiplexing (MDM) is a promising technique to increase the bandwidth density of optical channels dramatically, and when coupled with wavelength division multiplexing (WDM), could enable high-performance optical interconnects [1]. In MDM, a single wavelength carries multiple data streams encoded in the different spatial modes of a waveguide, offering an extra degree of freedom in fibers and integrated photonic platforms. However, coupling optical fibers and integrated waveguides is challenging due to the large mode mismatch between them [2], [3], [4]. To date, direct one-to-one coupling between higher order modes in a fiber and those in a high-index contrast waveguide has been a critical bottleneck to the adoption of MDM in data communication systems.

To realize a full MDM+WDM fiber-chip communication link, it is critical to address the fiber-chip coupling challenge. While there are some recent demonstrations of coupling between waveguides and few-mode fibers (FMF), scalability and coupling efficiency remain a challenge. Vertical coupling using gratings has been demonstrated [5], [6], [7], [8], [9],
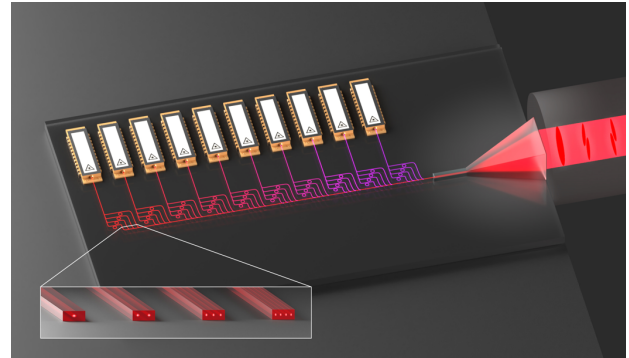
Fig. 1. Multimode chip to fiber interface concept showing a 3D polymer taper bridging the silicon waveguide and the multimode fiber integrated into an active photonic chip.

[10], and edge couplers have been designed and shown to enable Silicon-on-Insulator (SOI) waveguide mode conversion [11], [12], [13], [14], [15], [16], [17], [18]; in these demonstrations however, the demonstrated coupling efficiencies and operating bandwidths have been limited. We summarize different demonstrated approaches in Table S1. In this work, we experimentally demonstrate a platform for one-to-one high bandwidth edge coupling between higher-order modes of a silicon waveguide and those of a FMF.

II. DESIGN AND FABRICATION

Our design comprises an adiabatic multi-stage silicon inverse taper integrated with a low-index polymer waveguide [19], [20]. We design the taper to achieve the desired mode conversion in two stages, as shown in Fig. 2: the first converts the modes between a multi-mode (MM) Si waveguide and an intermediary rectangular polymer waveguide (Fig. S1); the second shapes the polymer modes both horizontally and vertically for efficient matching of the waveguide mode to a FMF mode (Fig. S2). Both stages consist of discretized tapers, where each sub-division is adiabatically tapered to guarantee one-to-one mode conversion. We achieve minimal crosstalk between the modes by slowly varying the Si waveguide width, increasing the degree of adiabaticity in sections along the Si-polymer structure where the modes hybridize, as proposed in great detail by Dai and Mao [11]. These mode hybridization regions, which arise from the waveguide's vertical asymmetry, are of special importance and become evident when plotting the supported modes' dispersion for varying waveguide widths. Once these regions are identified, a slow tapering between the waveguide widths just before and after each region will guarantee an efficient mode conversion. This means that each tapering stage corresponds to a different

Fig. 3. a) Schematic diagram of the device's top view. b) Optical microscopy of the silicon taper's tip buried under the straight polymer waveguide. c) End facet of our device showing the cross-section of the 3D polymer waveguide clad with NOA148. d) Optical microscopy (top-view) of our proposed chip-fiber interface where the 3D waveguide is aligned to the FMF core.
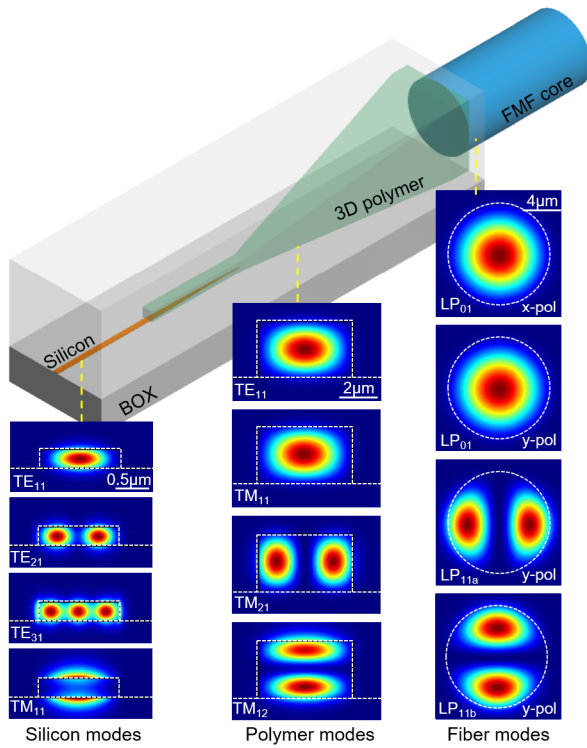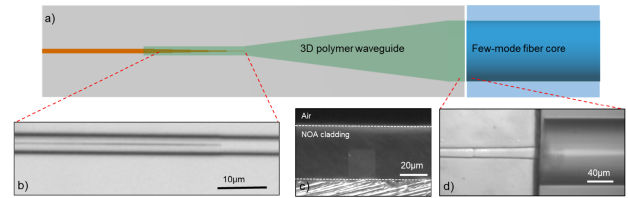

Fig. 2. Schematic diagram of our silicon to FMF mode converter. As a first stage, we convert the first 4 TE silicon waveguide modes to 4 different polymer modes via a multi-stage silicon taper buried under a straight polymer waveguide. In the second stage, we spatially expand the polymer modes in horizontal and vertical dimensions with a 3D polymer taper. One can see that the polymer modes match the FMF LP modes, and the polymer waveguide works as an intermediary between silicon and FMF modes.

for the polymer waveguide patterning. The SU-8 waveguide is patterned directly over the multi-stage silicon taper along its length using contact lithography. To pattern the 3D Ip-dip waveguide aligned to the SU-8 waveguide output, we use 3D nanolithography (Nanoscribe Photonic Professional GT) based on two-photon polymerization. We dice individual chips with a dicing saw and clad each of them with a 40 μm layer of NOA148 UV-curing optical adhesive ($n \approx 1.47$). We finally polish the chip facets using diamond lapping film (Fig. 3).

We design a set of adiabatic directional couplers to selectively excite the (TE_{11}, TE_{21}, TE_{31}, and TM_{11}) modes of a multimode 220×1200 nm^2 silicon waveguide [21], using single-mode waveguides (see Fig. S4 for details on the aforementioned directional couplers) with an external fiber-coupled tunable laser source (TLS). The excited modes are then converted one to one into the (TE_{11}, TM_{11}, TM_{21}, and TM_{12}) modes of a 3×5 μm^2 polymer (SU-8) waveguide and then resized with the 3D waveguide (Ip-dip) to a 22×23 μm^2 cross-section. The large polymer waveguide cross-section is then edge-coupled to the LP_{01} and LP_{11} modes of a FMF (Coherent FUD-3729 MM-GSF-20/125-10A, 20 μm core diameter, 4" long) as shown in Fig. 3 d). We image the excited fiber modes with a lens and an IR camera and extract the phase and amplitude profiles of the excited FMF modes through off-axis digital holography [22], [23].

III. RESULTS

Our mode conversion platform successfully excites the FMF modes expected from our design. In Figure 4, we show the simulated field intensity distribution of the expected fiber modes (2nd column) and compare them to the experimental LP modes imaged at the output facet of the fiber (3rd column). A polarization beam splitter was used to verify each mode's polarization. We show an average chip-to-fiber coupling efficiency of -4 dB for all modes and an average of -6.8 dB crosstalk between each mode and the next highest crosstalk one (Fig. 4 last column). We calculate this crosstalk between the experimental and simulated FMF modes by fitting the phase and amplitude profiles obtained from the off-axis holography technique (Fig. S5) to the expected fiber modes and solving for the superposition coefficients.

Additionally, we experimentally show an average multiplexing-demultiplexing crosstalk to the closest mode of -7 dB and a conversion efficiency of -14 dB for the silicon-polymer conversion stage. We measure this performance by fabricating two identical devices and placing

mode hybridization region. And in turn, mode conversion will happen at different propagation lengths through the multi-stage taper, as shown in Fig. S3. We simulate our structure using commercial software (MODE from Lumerical Inc.) and optimize our design for the parameters shown in Fig. S1. Our design converts one-to-one the first 3 TE modes and the fundamental TM mode of a MM silicon waveguide into the TE_{11}, TM_{11}, TM_{21}, TM_{12} modes of a polymer waveguide, respectively. These polymer waveguide modes efficiently match the LP_{01} and LP_{11} modes of a FMF (Fig. 2).

We demonstrate the mode converter on a 220nm SOI waveguide platform, with two additional lithography layers of SU-8 ($n \approx 1.57$) and Ip-dip ($n \approx 1.53$) that serve as the polymer waveguide core. The silicon waveguide layer is defined with e-beam lithography and fluorine-based ICP etching. We include silicon single-mode to higher-order mode adiabatic converters, which work with a SiO$_2$ cladding. In contrast, the silicon-to-polymer multi-stage tapers must be kept without cladding for further processing. We deposit and pattern a 40 nm thick Cr etch-stop layer on the areas that need to be air clad. We use e-beam deposition for the Cr and pattern it with a standard lift-off process. We then clad the whole sample with 2 μm of PECVD SiO$_2$ and pattern it with contact lithography for the cladding removal. We remove the SiO$_2$ cladding deposited on the Cr-covered areas with fluorine-based ICP etching. We remove the Cr using a wet etch. At this point, we have air-clad multi-stage tapers ready
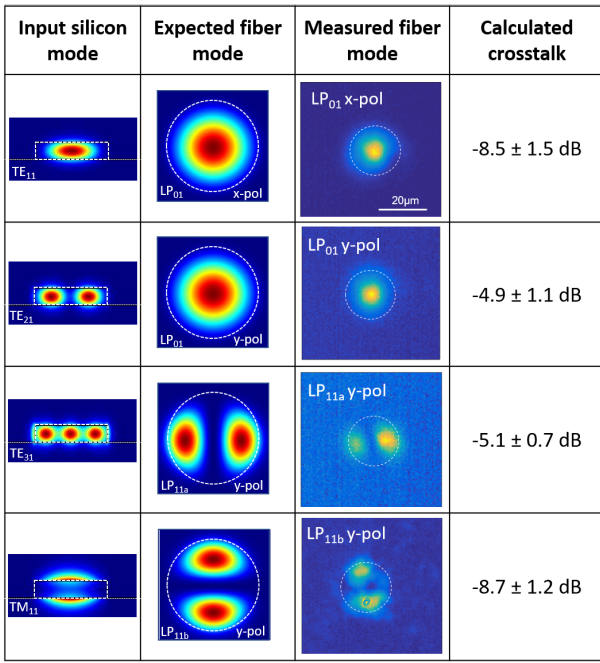
Fig. 4. Simulation of input higher order silicon waveguide modes (1st column), corresponding expected FMF modes (2nd column), and experimentally excited FMF modes (3rd column) using our mode converter. In the last column, we report the crosstalk between the expected mode and the highest crosstalk mode obtained from the off-axis holography technique.

TABLE I

CONVERSION EFFICIENCY FOR THE SILICON-POLYMER-SILICON FOUR MODE CONVERSION AT A WAVELENGTH OF 1550 NM. THE INPUT AND OUTPUT MODES WERE EXCITED AND RECOVERED THROUGH ADIABATIC DIRECTIONAL COUPLERS AND SINGLE-MODE SILICON WAVEGUIDES

In \ Out	TE_{11}	TE_{21}	TE_{31}	TM_{11}
TE_{11}	-11.24 ± 0.4 dB	-24.79 ± 0.7 dB	-23.41 ± 0.7 dB	-25.25 ± 2 dB
TE_{21}	-24 ± 0.6 dB	-14.48 ± 0.1 dB	-22.6 ± 2.4 dB	-21.62 ± 0.1 dB
TE_{31}	-26.4 ± 0.1 dB	-23.81 ± 0.1 dB	-18.03 ± 1 dB	-22.55 ± 0.8 dB
TM_{11}	-18.27 ± 0.9 dB	-21.95 ± 0.3 dB	-19.49 ± 0.3 dB	-14.57 ± 0.5 dB

them on the same chip front to front: one working as a mode multiplexer and the other as a mode demultiplexer (see Fig. S6). This setup allows us to individually excite with an external TLS each of the silicon higher order modes one at a time using the adiabatic directional couplers, convert it to a polymer mode, convert it back to a silicon mode, and measure its conversion efficiency and crosstalk to the off-diagonal modes with a fiber-coupled optical power meter (Table I).

Finally, we show the capability for terabit per second data transmission link based on the MDM +WDM using four wavelengths in the L-band range, forming 16 channels. Based on the same setup as in the previous paragraph (Fig. S6), we send a 16 Gb/s non-return-to-zero (NRZ) On-off keying (OOK) modulated signal through each of the four modes for the 1570.0 nm, 1573.3 nm, 1576.2 nm, and 1582.0 nm wavelength channels of the DWDM ITU Grid specification for L-band with 50 GHz spacing [32]. We show error-free transmission of 16 Gb/sec per channel by measuring bit error rate (BER) values using a pseudorandom binary sequence (PRBS31) as the test platform (Fig. 5). From these
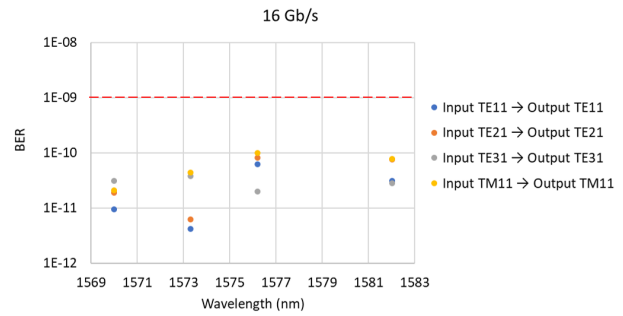

Fig. 5. WDM+MDM BER measurement for 4 silicon modes converted into a polymer waveguide and back into silicon.

measurements, we can infer that our device can transmit error-free 16 Gb/s signals in all four guided modes for each of the 30 channels on the L-band DWDM ITU 50 GHz grid between 1570 nm and 1582 nm, spanning a spectral range of 1.45 THz. With 30 carrier wavelengths, transmitting on four modes each, at 16 Gb/s/channel amounts to a total data transmission capability of 1.92Tb/s, with the worst modal crosstalk less than −6 dB (see Fig.S7).

IV. CONCLUSION

Our work paves the way for an efficient and scalable solution for the interface between on-chip silicon MDM devices and FMF. Our integrated platform is capable of directly coupling to a FMF the higher order modes used for on-chip data processing. We demonstrate a MDM+WDM-compatible design capable of one-to-one conversion between four modes of an integrated multimode silicon waveguide and four LP modes of a FMF. The platform is limited only by chip footprint and fabrication tolerances. Developing a single material polymer waveguide and techniques such as nonlinear adiabatic tapering are to be explored to reduce the taper length, relax the fabrication constraints and improve our device performance regarding conversion efficiency and crosstalk suppression. Our work shows a straightforward path to further scaling the data rate of WDM schemes, such as [24], by the multiplicative scaling given by the number of modes times the number of wavelengths.

REFERENCES

[1] L.-W. Luo et al., "WDM-compatible mode-division multiplexing on a silicon chip," *Nature Commun.*, vol. 5, no. 1, pp. 1–7, Jan. 2014. [Online]. Available: https://www.nature.com/articles/ncomms4069

[2] Y. Su, Y. He, H. Chen, X. Li, and G. Li, "Perspective on mode-division multiplexing," *Appl. Phys. Lett.*, vol. 118, no. 20, May 2021. [Online]. Available: https://aip.scitation.org/doi/10.1063/5.0046071

[3] B. Stern et al., "On-chip mode-division multiplexing switch," *Optica*, vol. 2, no. 6, p. 530, Jun. 2015.

[4] H. Huang et al., "Demonstration of terabit coherent on-chip optical interconnects employing mode-division multiplexing," *Opt. Lett.*, vol. 46, no. 10, p. 2292, May 2021. [Online]. Available: https://www.osapublishing.org/ol/abstract.cfm?doi=10.1364/OL.424727

[5] T. Watanabe, B. I. Bitachon, J. Leuthold, B. Baeuerle, P. Ma, and Y. Fedoryshyn, "Coherent few mode demultiplexer realized as a 2D grating coupler array in silicon," *Opt. Exp.*, vol. 28, no. 24, pp. 36009–36019, 2020. [Online]. Available: https://www.osapublishing. org/oe/abstract.cfm?uri=oe-28-24-36009

[6] J. M. Baumann et al., "Silicon chip-to-chip mode-division multiplexing," in *Proc. Opt. Fiber Commun. Conf. Expo. (OFC)*, Mar. 2018, pp. 1–3. [Online]. Available: https://www.osapublishing. org/abstract.cfm?uri=OFC-2018-W1E.4

[7] Y. Tong, W. Zhou, X. Wu, and H. K. Tsang, "Efficient mode multiplexer for few-mode fibers using integrated silicon-on-insulator waveguide grating coupler," *IEEE J. Quantum Electron.*, vol. 56, no. 1, pp. 1–7, Feb. 2020.

[8] Y. Lai, Y. Yu, S. Fu, J. Xu, P. P. Shum, and X. Zhang, "Compact double-part grating coupler for higher-order mode coupling," *Opt. Lett.*, vol. 43, no. 13, p. 3172, Jul. 2018. [Online]. Available: https://www.osapublishing.org/abstract.cfm?URI=ol-43-13-3172

[9] D. Garcia-Rodriguez, J. L. Corral, A. Griol, and R. Llorente, "Bimodal grating coupler design on SOI technology for mode division multiplexing at 1550 nm," *Opt. Exp.*, vol. 26, no. 15, pp. 19445–19455, Jul. 2018. [Online]. Available: https://www.osapublishing. org/oe/abstract.cfm?uri=oe-26-15-19445

[10] J. L. P. Ruiz et al., "Efficient integrated tri-modal coupler for few-mode fibers," *Opt. Exp.*, vol. 30, no. 2, pp. 2539–2546, Jan. 2022. [Online]. Available: https://www.osapublishing.org/oe/abstract.cfm?uri=oe-30-2-2539

[11] D. Dai and M. Mao, "Mode converter based on an inverse taper for multimode silicon nanophotonic integrated circuits," *Optics Exp.*, vol. 23, no. 22, pp. 28376–28388, Nov. 2015. [Online]. Available: https://www.osapublishing.org/oe/abstract.cfm?uri=oe-23-22-28376

[12] J. Zhu, H. Huang, Y. Zhao, Y. Li, Z. Sheng, and F. Gan, "Efficient silicon integrated four-mode edge coupler for few-mode fiber coupling," *Chin. Opt. Lett.*, vol. 20, no. 1, 2022, Art. no. 011302. [Online]. Available: https://www.researching.cn/articles/OJf5ededc456286ded/html

[13] X. Cao, K. Li, Y. Wan, and J. Wang, "Efficient mode coupling between a few-mode fiber and multi-mode photonic chip with low crosstalk," *Opt. Exp.*, vol. 30, no. 13, pp. 22637–22648, Jun. 2022. [Online]. Available: https://opg.optica.org/oe/abstract.cfm?uri=oe-30-13-22637

[14] W. Shen, J. Du, J. Xiong, L. Ma, and Z. He, "Silicon-integrated dual-mode fiber-to-chip edge coupler for 2 × 100 Gbps/lambda MDM optical interconnection," *Opt. Exp.*, vol. 28, no. 22, p. 33254, Oct. 2020. [Online]. Available: https://www.osapublishing. org/abstract.cfm?URI=oe-28-22-33254

[15] L. Cheng, S. Mao, Z. Chen, Y. Wang, C. Zhao, and H. Y. Fu, "Ultra-compact dual-mode mode-size converter for silicon photonic few-mode fiber interfaces," *Opt. Exp.*, vol. 29, no. 21, pp. 33728–33740, Oct. 2021. [Online]. Available: https://www.osapublishing. org/oe/abstract.cfm?uri=oe-29-21-33728

[16] Y. Lai, Y. Yu, S. Fu, J. Xu, P. P. Shum, and X. Zhang, "Efficient spot size converter for higher-order mode fiber-chip coupling," *Opt. Lett.*, vol. 42, no. 18, pp. 3702–3705, Sep. 2017. [Online]. Available: https://opg.optica.org/ol/abstract.cfm?uri=ol-42-18-3702

[17] X. Yi, W. Zhao, Y. Shi, and D. Dai, "Novel concept of high-efficiency coupling between silicon photonic chips and few-mode-fibers," in *Proc. Asia Commun. Photon. Conf. (ACP)*, Nov. 2022, pp. 1600–1602.

[18] K. Li, X. Cao, and J. Wang, "Broadband and efficient multi-mode fiber-chip edge coupler on a silicon platform assisted with a nano-slot waveguide," *Opt. Exp.*, vol. 30, no. 26, pp. 47249–47263, Dec. 2022. [Online]. Available: https://opg.optica.org/oe/abstract.cfm?uri=oe-30-26-47249

[19] O. A. J. Gordillo, U. D. Dave, and M. Lipson, "Bridging between Si and few-mode fiber higher order modes," in *Proc. Conf. Lasers Electro-Optics (CLEO)*, May 2020, pp. 1–2. [Online]. Available: https://www.osapublishing.org/abstract.cfm?uri=CLEO_SI-2020-SM2O.6

[20] O. A. J. Gordillo, U. D. Dave, and M. Lipson, "One-to-one coupling higher order modes in a fiber to higher order modes in silicon waveguide," in *Proc. Conf. Lasers Electro-Optics (CLEO)*, May 2021, pp. 1–2. [Online]. Available: https://www.osapublishing. org/abstract.cfm?uri=CLEO_SI-2021-SW3C.4

[21] U. D. Dave and M. Lipson, "Efficient conversion to very high order modes in silicon waveguides," in *Proc. Conf. Lasers Electro-Optics (CLEO)*, San Jose, CA, USA, May 2019, pp. 1–2. [Online]. Available: https://www.osapublishing.org/abstract.cfm?URI=CLEO_SI-2019-SM3J.6

[22] E. Cuche, P. Marquet, and C. Depeursinge, "Spatial filtering for zero-order and twin-image elimination in digital off-axis holography," *Appl. Opt.*, vol. 39, no. 23, pp. 4070–4075, 2000. [Online]. Available: https://www.osapublishing.org/ao/abstract.cfm?uri=ao-39-23-4070

[23] S. van der Heide et al., "Optical field characterization using off-axis digital holography," in *Proc. Opt. Fiber Commun. Conf. Exhib. (OFC)*, Mar. 2022, pp. 1–3. [Online]. Available: https://opg.optica.org/abstract.cfm?uri=OFC-2022-M3Z.6

[24] A. Rizzo et al., "Integrated Kerr frequency comb-driven silicon photonic transmitter," 2021, *arXiv:2109.10297*.